NOAA Technical Memorandum OAR ARL-284
https://doi.org/10.25923/fyjf-q832

The Western WRF Modeling Project: System Design and Model Evaluation

Fong Ngan[1,2]
Mark Cohen[1]
Sonny Zinn[1]
Weifeng Jiang[1]
Hongfeng Shen[4]
HyunCheol Kim[1,2]
Walter Schalk[3]

October 2022

National Oceanic and Atmospheric Administration
Office of Oceanic and Atmospheric Research
Air Resources Laboratory

1 NOAA/Air Resources Laboratory, 5830 University Research Court, College Park, MD
2 Cooperative Institute for Satellite Earth System Studies, College Park, MD
3 NOAA/Air Resources Laboratory, Special Operations & Research Division, Las Vegas, NV
4 Contractor, ERT, Inc., 14401 Sweitzer Lane, Suite 300, Laurel, MD

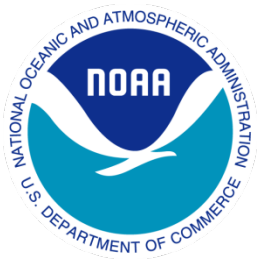

NOAA Technical Memorandum OAR ARL-284
https://doi.org/10.25923/fyjf-q832

The Western WRF Modeling Project: System Design and Model Evaluation

By Fong Ngan, Mark Cohen, Sonny Zinn, Weifeng Jiang, Hongfeng Shen, HyunCheol Kim and Walter Schalk

October 2022

National Oceanic and Atmospheric Administration
Oceanic and Atmospheric Research
Air Resources Laboratory

U.S. Department of Commerce
Secretary of Commerce Gina Raimondo

Under Secretary for Oceans and Atmosphere/NOAA Administrator
Dr. Richard W. Spinrad

Assistant Secretary for Oceans and Atmosphere/Deputy NOAA Administrator
Janet Coit

Abstract

An operational WRF modeling system was developed to provide forecasts for daily operations, special experimental support, and emergency response components of the NOAA Air Resources Laboratory (ARL) Special Operations and Research Division (SORD) missions. It serves as a coupling platform of modeling and measurements for the understanding of planetary boundary layer (PBL) dynamics, with attention to particular aspects of atmospheric fluid flow that impact the transport and dispersion of pollutants. In addition, the system is a testbed for ARL research projects such as general PBL parameterizations, direct mesonet data inclusion and other data assimilation approaches, and desert climate studies. The system has been operating since May 2021 to produce a 4-day forecast four times per day, at 00, 06, 12, and 18 UTC. WRF meteorological data, HYSPLIT-formatted meteorological files, and graphics are generated and distributed to ARL/SORD for their daily use. A web application (https://apps.arl.noaa.gov/wrff) was implemented to display the graphics. One-year forecast results (May 1st, 2021 – April 30th, 2022) have been evaluated with the mesonet data operated by ARL/SORD in Las Vegas, NV and Idaho Falls, Idaho and radiosonde data. The mean absolute error (MAE) in surface temperature, wind speed and wind direction shows that during the winter and early spring, the Idaho domain had larger biases than in other months of the year. The daily MAE increases slightly from forecast day 1 to day 4. The forecast for the Idaho domain (ID) has larger biases than the Nevada domain (NV). The MAE computed for the most highly resolved inner domain ranged from 2.1 – 2.3 (NV) and 2.9 – 3.3 (ID) degrees Celsius for surface temperature, 1.5 – 1.7 (NV) and 1.8 – 2.0 (ID) ms^{-1} for wind speed, and 41 – 44 (NV) and 52 – 57 (ID) degrees for wind direction, with the higher end of the ranges generally corresponding to longer forecast periods (i.e., days 3 and 4). The evaluation with radiosonde data shows that the MAE of temperature is larger in the PBL and gradually decreases with height in the free troposphere, and the MAE of wind direction is larger near the surface and rapidly decreases with height. For wind speed, similar model errors are present at the levels of 1 – 4 km and then gradually increase with altitude above PBL.

Table of Contents

List of Figures

List of Tables

1.0 Introduction

NOAA Air Resources Laboratory (ARL) Special Operations and Research Division (SORD) has been working with the Department of Energy since 1949. Through Interagency Agreements, SORD provides a comprehensive atmospheric sciences program of basic and applied meteorological research to support a wide variety of projects, experiments, and programs conducted under the management of the Department of Energy (DOE) and the DOE/National Nuclear Security Administration (NNSA). This work is conducted at the Nevada National Security Site (NNSS) in southern Nevada and the Idaho National Laboratory (INL) in southeastern Idaho. A component of this work is to provide near-real time meteorological data to these sites. SORD operates and maintains a 24 station mesonet in southern Nevada (Randerson 1999; Randerson and Sanders, 2002) and a 34 station mesonet in southeastern Idaho (Clawson et al. 2018). In addition, specialized site forecasts are prepared for daily operations, special experiment support, and emergency response activities at these sites. This information is critical to the field operations of the DOE and NNSA sites, where precision forecasts are needed in order to conduct non-proliferation national security research. An operational meteorological modeling system can provide these forecasts as well as provide the basis for ARL research projects such as general model parameterizations, direct mesonet data inclusion, and desert climate parameterizations.

The NOAA ARL HYSPLIT model (Stein et al., 2015) is one of the most extensively used atmospheric transport and dispersion models in the atmospheric sciences community, including widespread operational emergency-response applications to assess the movement of harmful materials in the atmosphere. Efforts to quantify and reduce uncertainties in HYSPLIT simulations are essential, including an assessment of uncertainties in the numerical weather prediction data that are used to drive dispersion simulations. Evaluating meteorological variables, such as wind, stability, and mixing variables relevant to the transport and dispersion of pollutants is fundamental to assessing the performance of numerical weather prediction models and the dispersion simulations driven by the meteorological model data. The development of an operational modeling testbed for the regions surrounding ARL/SORD in Las Vegas, Nevada and Idaho Falls, Idaho is an opportunity to perform significant model evaluations as the regions contain well-established meteorological mesonet observations. This system will use the mesonet data to evaluate and improve local and regional meteorological modeling of PBL dynamics, with attention to particular aspects of atmospheric fluid flow that impact the transport and dispersion of pollutants.

We use the Advanced Research dynamic core of the Weather Research and Forecasting (WRF; Powers et al., 2017) as the meteorological model to build the platform for forecasts and model evaluation against mesonet data, focusing on the model components that impact the movement of pollutants in the atmosphere. A WRF forecasting system has been developed to run four cycles per day (00z, 06z, 12z, and 18z), each producing a 4-day forecast. WRF meteorological data,

HYSPLIT-formatted meteorological files and graphics are generated and distributed to support ARL/SORD in their critical emergency response functions. The operation of this system is critical; thus, a backup server has been installed in the event of an operational failure. The backup server will also be the primary research server where model parameterizations, direct mesonet data inclusion and other data assimilation approaches, and desert climate phenomena will be studied. Besides the importance of this system to provide critical weather data and information to the DOE and NNSA, the coupling of modeling and measurements is a platform to increase understanding of PBL dynamics to improve numerical weather and transport and dispersion predictions.

2.0 The Setup of the WRF Forecasting System

2.1 Operating machines

The main operating machine for the WRF forecast is "westwrf1.arl.noaa.gov" while the backup server is "westwrf2.arl.noaa.gov". Both machines are identical in their environmental setup, software, and directory structures. All the codes and scripts are developed and tested on the main operating machine. They are stored and backed up on GitHub, and then the backup server obtains the forecasting package through "git clone". We use gfortran and mpich as the compiler to install WRF version 4.2.2 and HYSPLIT version 5.1.0. Required software and libraries are NetCDF, IDL, NCL, imagemagick, crontab, and csh scripts. The output files are uploaded to the FTP servers westwrf01@ftp.arl.noaa.gov (in directory /pub/WRF01/data-NV[ID]) and westwrf02@ftparl.noaa.gov (in directory /pub/WRF02/data-NV[ID]) for users to access the forecast data. Note that only one day's output is kept on the FTP servers. The machines are occasionally rebooted for maintenance purposes. The rebooting windows are 11:00 and 17:00 Eastern Time. The two machines are rebooted at different times to keep at least one machine in operation at any given time.

2.2 Operating schedules

The forecasting system runs two sets of nested, inner domains for the Nevada area (NV) and Idaho area (ID). The inner domains share the same outer domain (D01), with 18-km horizontal grid spacing (shown in Section 3, Figure 5). NOAA's operational Global Forecast System (GFS) meteorological forecast model product in 0.5-degree spatial resolution is used to initialize WRF. We access the data via the NOAA Operational Model Archive and Distribution System (NOMADS; Rutledge et al. 2006). The operating schedule is shown in Figure 1. Each cycle runs for 102 hours including a 6-hour spin up. For example, the 00z cycle of the NV domain starts at 00:15 am and completes between 3:30 – 4:30 am. The run for the ID domain starts 40 minutes later (at 00:55 am) to wait for the completion of the GFS download and the simulation for domain D01. The cycle run finishes between 4:10 - 5:10 am. Note that forecasts and evaluations

use Coordinated Universal Time (UTC). The cron-jobs are scheduled using the Eastern Time zone (Figure 1) which has a one hour difference between daylight saving time (UTC-4) and standard time (UTC-5).

2.3 Overview of the run scripts

Two main scripts were developed for the WRF forecasting system (Figure 2). The "run.NV.csh" (and "run.ID.csh") carries out the following four steps to generate WRF and HYSPLIT files:

- Download GFS 0.5 degree data (labeled as "gfs")
  If the download of GFS data fails (checked by run.gfs.csh), the script will launch a backup run using the latest available GFS data.
  The directory to store GFS files is "ini-data".
- Run the WRF preprocessing system (labeled as "wps")
  The directory to keep WPS files is "wps-out".
- Execute WRF for domain D01 (only run once, and used for both local/regional forecasts), D02, and D03 (labeled as "wd1", "wd2", and "wd3")
  The output directory for WRF files is "wrf-out".
- Run arw2arl to convert WRF output to HYSPLIT meteorological format
  The output directory for HYSPLIT meteorological format files is "arl-out".

Note that each backup run has its own subdirectories, following the naming convention as bakrun-[NV or ID]-YYYYMMDD[cycle]z. A backup run will be terminated when the NV-D01 simulation of the next cycle starts (i.e., a successful download of GFS data), to ensure there are sufficient computational resources for the next operational cycle.

The "run.check.csh" runs the following post-processing steps (Figure 2):

- Check the log file and email messages for a completed cycle or a failed job
- List missing cycles (run.chkcyc)
- Generate figures and trajectories (described in Section 4) using following scripts:
  run.ncl – surface and upper-level NCL graphics
  run.precip – 1-hr, 3-hr, and 24-hr precipitation graphics
  run.tswrf – meteograms and wind profile plots
  run.traj – trajectory figures
  The output directories for graphics and trajectories are "png-out" and "traj-out".
- Reduce archived WRF file size by only keeping a small set of variables
- Delete intermediate files
- Transfer output files to the FTP servers.

To reduce disk usage, intermediate files, such as the GFS data and WPS files are deleted once the cycle run is completed. The post-processing script also reduce the size of WRF files (with suffix "-cut") by only keeping the variables described in Table 1.

The list of directories for NV domain on westwrf1.arl.noaa.gov:

Running directory	/data/fantinen/WRF/auto-WRF-NV
Output	/data/fantinen/data-NV

The list of directories for ID domain:

Running directory	/data/fantinen/WRF/auto-WRF-ID
Output	/data/fantinen/data-ID

The system is currently run under an account "fantinen" and in its home directory. Eventually, it will be moved to a system-owned account and directory without depending on any one person. For the storage of output files, the directory follows the naming convention as YYYYMMDD[cycle]z. Once the simulation is complete, the "wrf-out" and "arl-out" directories are moved to the storage directory while other two sub-directories ("ini-data" and "wps-out") for intermediate files are deleted (Figure 2). Then, the post-processing script generates the "png-out" and "traj-out" directories for graphics and trajectory files. Note that the same directory structure is applied to the backup server (westwrf2.arl.noaa.gov).

As for disk usage, the NV and ID simulations take 17 GB and 15 GB per cycle (i.e., 68 GB and 60 GB per day), respectively. We free up disk space by deleting WRF files for the coarse domains every three months. By only keeping output for the inner-most domains (NV03 and ID03), it reduces the disk usage to 11 GB per cycle (i.e., 44 GB per day). Then, we further remove the "wrf-out" directory every six-nine months to have sufficient disk storage for continued operations. The "arl-out" and "png-out" directories are kept and they take about 3 GB per cycle (i.e., 12 GB per day). When the system accumulates multiple-year forecasts, we expect to delete the remaining directories to free up more disk space.

2.4 Operation overview

Figure 3 and Figure 4 show the time series of the processing time for each cycle from May 1st, 2021 to April 30th, 2022 for the NV and ID domains, respectively. The operation for the ID domain started on May 12th, 2021. Some missing or incomplete cycles (red dots in Figure 3a and Figure 4a) are due to testing-related interruptions, schedule adjustments, and GFS download failure. The most significant cause for forecasts failures is the availability of GFS files that are used to initialize the WRF simulation. The download failure may be due to the NOMADS FTP connection issue, the heavy traffic slowing down the download, or a delay in the operational

production of GFS files. Since the start of the operation in May 2021, the GFS downloading issue has happened three times (October 3rd, 2021, January 4th, 2022, August 23rd and 26, 2022), interrupting multiple operational cycles in a row. We modified the scripts and added backup runs to make the system more resilient to these types of issues.

As shown in Figure 3 and Figure 4, each cycle takes about 3-4.5 hours to complete, using 24 CPUs. The total processing time depends on the amount of time for running the inner-most domain (wd3), which varies between 90 - 150 minutes. For other components, the processing times are quite consistent. The GFS download takes about 7 – 14 minutes. The coarse domain (wd1) needs about 30 minutes to complete, while the middle domain (wd2) takes 50 - 60 minutes. Note that the ID domain uses the wd1 output from the NV domain run. In general, the wd3 for the ID simulation runs about 20-30 minutes longer than the wd3 of the NV domain. Starting in mid-November, we switched to using 36 CPUs for the WRF simulation, which shortened the processing time by about 20-30 minutes. Using more CPUs may not speed up the WRF simulation. The current setting, 36 CPUs, is the maximum number of processors according to the domain configuration used in this forecasting system.

The increase in processing time in mid-April 2022 was due to turning on the diagnostic option in WRF (nwp_diagnostics=1). This option causes WRF to write out additional diagnostic variables, such as max wind speed, updraft velocity, downdraft velocity, etc. Details regarding this option are available at http://www2.mmm.ucar.edu/wrf/users/docs/AFWA_Diagnostics_in_WRF.pdf. However, this diagnostic mode requires significantly more computational resources. The WRF codes relevant for generating the diagnostic variables were modified to only compute and write out the maximum wind speed – the key parameter needed – to minimize the extra processing time. The running time to complete the forecast became similar to prior operations once the modification of the WRF code was implemented.

3.0 Model Configuration

The WRF model (version 4.2.2) is configured with two sets of domains (Figure 5 and Table 2) that share the outer domain (D01). The projection center is at 36.67°N and 115.75°W with standard latitude at 36.67°N and 42.67°N. We use 33 vertical layers, with the highest resolution near the surface and 100 hPa for the model top. The thickness of the lowest layer is around 16 m, and 20 layers are included below 850 hPa (~1.5km). Table 3 summarizes the physics options used in the WRF forecasting system. The simulations are initialized by the GFS data in 0.5 degree spatial resolution and 3-hour temporal resolution. The installation of the WRF model is in /data/fantinen/WRF/wrf_v4.2.2.

HYSPLIT version 5.1.0 is installed in /data/fantinen/HYSPLIT/hysplit.v5.1.0. This is used for converting the WRF output files to HYSPLIT-ready meteorological format and to run trajectory and dispersion simulations if necessary.

4.0 Graphics Display

Graphics are generated using NCAR Command Language (NCL, 2019). A web application is implemented to display the graphics (https://apps.arl.noaa.gov/wrff/). The shapefiles of the NNSS and INL facilities are overlaid on the graphics to display their locations in the model domain. Available figures are listed below:

- Surface plots (Figure 6 and Figure 7) – hourly figures (i.e., for all 96 hours of each forecast), for all three domains, and zoom-in plots for the local areas of NNSS and INL. There are 12 surface figures for each forecast hour including:
  Total cloud fraction
  Cloud water mixing ratio (1st model layer)
  Snow depth
  Precipitable water
  2-m temperature
  Total precipitation accumulation
  Reflectivity
  10-m wind speed and wind barb
  10-m maximum wind speed and 10-m wind barb
  1-hour precipitation (every hour)
  3-hour precipitation (every 3 hours)
  24-hour precipitation (every 24-hours)

- Upper level plots (Figure 8) – hourly figures and for all three domains. Four upper-level graphics are:
  850 mb weather map (temperature, geopotential height, and wind)
  750 mb weather map
  300 mb weather map (absolute vorticity, geopotential height, and wind)
  300 mb weather map (geopotential height and wind)

- Skew-T diagram (Figure 9) – available every 6 hours at 00, 06, 12, and 18 UTC and for all three domains.
  Available stations for graphics are listed in Table 3.

- Meteograms (Figure 10) – for inner-most domains (NV03 and ID03) including time series plots of the following meteorological parameters: 2-m relative humility, 2-m temperature, 10-m wind speed, 10-m wind barb, and 1-hour precipitation.

- Time series plot of wind profile (Figure 11).

5.0 Model Evaluation

5.1 Model evaluation using mesonet data

Statistical metrics have been computed for WRF forecast results for one year's forecast (from May 1st, 2021 to April 30th, 2022) by comparison against the mesonet wind and temperature measurements. The observational data are obtained from https://download.synopticdata.com. Figure 5, Table 5, and Table 6 show the mesonet locations in Nevada and Idaho. The evaluation in this report did not use station A12AI, COX, and CFA (highlighted in grey in the tables) because the data were not downloaded probably. The mesonet data reporting frequency is 15 minutes and 5 minutes for the Nevada and Idaho mesonet, respectively, while the WRF model output is hourly. We use the 15 minute average at the top of the hour to evaluate the hourly WRF results. Figure 12 is the mean absolute error (MAE) for each forecast during this year-long evaluation period (102 hour forecast per cycle and four cycles per day). The color-coded dots are for the WRF forecast from different domains. The MAE of each cycle ranges from 1 – 3 (up to 4 for the ID domain) ms^{-1} for wind speed, 30 – 60 (up to 80 for the ID domain) degrees for wind direction, and 1 – 3 (up to 8 for the ID domain) degrees Celsius for temperature. During the winter and early spring, surface temperatures in the ID domain had much larger biases than in other months of the year.

We selected eight days to compare the forecast of each day's 00z cycle with mesonet data at different locations. Figure 13 and Figure 14 show the time series of surface wind speed and wind barbs, respectively. The black lines and barbs are observations, while the other colors are model forecast winds from the inner-most domain (2-km grid spacing) during the July 1st – 8th time period. In general, model-predicted winds matched quite well with the observed winds. On July 3rd during 15 – 21 UTC), the July 1st 00z forecast (red line) under-predicted the maximum wind speed in the afternoon. The July 2nd 00z and July 3rd 00z forecast (blue and green lines) had smaller wind speed biases than the July 1st 00z forecast. One would expect that for any given forecast, it would start to diverge more from the observations as it made its way through its 102 hour duration. The model predicted the change of wind direction in the NV domain (station A22AD) reasonably well during this period. The model wind direction had more significant biases in the ID domain than the NV domain. Furthermore, on July 3rd during 00 – 09 UTC, the July 3rd forecast (green wind barbs) had improved wind direction predictions compared to the forecast from the previous two days (red and blue wind barbs).

We computed the MAE of the 2-km domain (NV03 and ID03) WRF results and mesonet data for forecast days one through four for the one year evaluation period (Figure 15). In general, biases increase slightly from day one to day four, as would be expected. The bias increase with forecast hours is less evident in the wind speed than the in other two variables. More significant biases are observed in the Idaho domain than in the Nevada domain. Note that the more complex terrain in the ID region may cause larger biases in the WRF forecast. The MAE associated with the

different forecast days ranged between 2.1 – 2.3 (NV03) and 2.9 – 3.3 (ID03) degrees Celsius for temperature, 1.5 – 1.7 (NV03) and 1.8 – 2.0 (ID03) ms-1 for wind speed, and 41 – 44 (NV03) and 52 – 57 (ID03) degrees for wind direction. Zhang et al. (2013) evaluated WRF forecasting results over a complex terrain region in Utah and the adjacent states for a one month period in Fall 2011, reporting the MAE for temperature 1.5 – 3.0 degrees Celsius, wind speed 1.2 – 1.9 ms^{-1}, and wind direction 38 – 60 degrees. Note that the statistics were computed for 2-day forecasts and one month period, using only observations in the Dugway Proving Ground, Utah area. The western WRF forecast presented in this study has similar model bias.

Probability density histograms for mesonet observations and model outputs are shown in Figure 16. The observed and model wind speed distribution have a good agreement for the NV domain. For the ID domain results, the model distribution of wind speeds is narrower than the observed distribution, with less forecasted values for wind speed larger than 3 ms^{-1} and more predicted values for lower wind speed. Also, the observed wind is underpredicted in the upper tail of the wind speed distribution. For wind direction distributions, the forecast has more southerly (180 – 210 degrees) and less northeasterly (20 – 70 degrees) than the observations in the NV domain. The comparison of the ID domain shows that the model produces more northeasterly (10 – 60 degrees) components of wind direction than the mesonet data. The temperature distributions of WRF match well with the observed distributions, except the model underpredicts the low extreme values and overpredicts the high extreme values in the ID domain.

Figure 17 and Figure 18 show the mean absolute error and mean bias at each mesonet station. During the one-year evaluation period, the forecast has a larger MAE at the stations in the eastern and southern parts of the mesonet network in the NV domain. The model overpredicts temperature at stations in the valley and wind speed at stations in higher terrain (Figure 18). For the ID domain, the spatial pattern of model error differs for temperature and wind. Wind speed and direction have smaller errors at stations in at lower elevations (the southern portion of the ID network). The temperature has larger errors in both eastern and southern parts of the ID network. Negative biases are present at most of the stations across the ID mesonet network for temperature and wind speed (Figure 18).

5.2 Model evaluations using radiosonde data

For the model evaluation of forecasts above the surface, we used the radiosonde station (VEF; shown in Figure 5) in the NV03 domain. The sounding data are available twice daily at 00 and 12 UTC and were downloaded from http://weather.uwyo.edu/upperair/sounding.html. The mean absolute error is computed from the sounding and one year's WRF forecast output from May 1st, 2021 to April 30th, 2022 (Figure 19). The model error decreases with increasing elevation for temperature and wind direction, with larger biases in the PBL and smaller biases in the free troposphere. The MAE for temperature is 5 – 6 degrees Celsius in the lowest 2 km. The MAE for wind direction varies greatly, ranging from 35 – 65 degrees, in the lowest 2 km. A similar model error in wind speed is present at the height of 1 – 4 km (about 2.5 ms-1 for MAE) and then

gradually increases with increasing altitude. A larger bias for wind speed, about 3 ms^{-1}, is presents at the height of 0.7 km.

6.0 Summary

A WRF forecasting system has been successfully implemented to provide forecasts, graphic output, and HYSPLIT-formatted meteorological files to support the daily operation at the ARL/SORD in Nevada and in Idaho). A coupling of modeling and measurements provides a platform to increase understanding of PBL dynamics, with attention to particular aspects of atmospheric fluid flow that impact the transport and dispersion of pollutants. Two sets of model domains with the finest horizontal resolution of 2 km cover the mesonet sites in Nevada and Idaho using the same outer domain with 18-km grid spacing. The simulations are initialized by using NOAA's operational GFS forecast data with a 0.5-degree spatial resolution. The system has been operating since May 2021 to produce four-day forecasts with four cycles (at 00, 06, 12, and 18 UTC) per day. Each cycle takes about 3 – 4.5 hours to complete. The total processing time depends primarily on the running time of the inner-most domain, while the running time for other steps is relatively consistent. The GFS download failure due to FTP connection issues and delays in the availability of GFS files is the primary cause of occasional incomplete forecasts. A web application was implemented to display the graphics (https://apps.arl.noaa.gov/wrff/), including surface plots, upper-level weather maps, skew-t diagrams, and meteogram figures.

One year of forecast results (from May 1st, 2021 to April 30th, 2022) were evaluated by comparison against the mesonet data operated by ARL/SORD. The mean absolute error (MAE) for each cycle shows that during the winter and early spring, surface temperatures in the ID domain had much larger biases than in other months of the year. The daily MAE increases slightly from forecast day 1 to day 4. In general, the forecast for the Idaho area has larger biases than the Nevada domain due to the more complex terrain in the ID region. The MAE computed for the inner-most domain (NV03 and ID03) ranged from 2.1 – 2.3 (NV03) and 2.9 – 3.3 (ID03) degrees Celsius for temperature, 1.5 – 1.7 (NV03) and 1.8 – 2.0 (ID03) ms^{-1} for wind speed, and 41 – 44 (NV03) and 52 – 57 (ID03) degrees for wind direction over days 1 through 4 of the forecasts. Similar WRF errors were found in an evaluation in complex terrain in Utah.

The probability density histograms for mesonet observations and model outputs show that the forecast for the NV domain captures the surface wind speed distribution well. However, in the ID domain, the model predicts more low wind speed (2 ms^{-1} and lower) and less medium and high wind speed (4 ms-1 and higher) compared to the observations. For the surface wind-direction distributions, the ID domain forecast has more easterly wind than the mesonet data, while the NV domain forecast has more southerly wind and less easterly wind than the observations. For surface temperature, the model underpredicts (overpredicts) the lower tail of the distribution that is lower (higher) than the observed distribution for the NV (ID) domain.

Regarding the spatial bias pattern, positive biases for temperature are present at stations in the valley of the NV domain (eastern part of the mesonet) and for wind speed at stations in the high terrain area (northern part of the network). Negative biases are present at most stations across the mesonet network in the ID domain for temperature and wind speed.

Radiosonde data at the VEF station are used to evaluate the model's performance for upper levels in the atmosphere. The MAE of temperature is larger in the PBL and gradually decreases with height in the free troposphere, and the MAE of wind direction is larger near the surface and rapidly decreases with height. For wind speed, similar model errors are present at the levels of 1 – 4 km and then gradually increase with altitude above PBL.

7.0 References

Chen, F., Dudhia, J., 2001: Coupling and advanced land surface–hydrology model with the Penn State–NCAR MM5 modeling system. Part I: model implementation and sensitivity. Mon. Wea. Rev. 129, 569–585.

Clawson, K. L., J.D. Rich, R.M. Eckman, N.F. Hukari, D. Finn, B.R. Reese, 2018: Climatography of the Idaho National Laboratory 4th Edition. NOAA Tech Memo OAR ARL-278. 322 pp.

Deng, A., Stauffer, D., Gaudet, B., Dudhia, J., Hacker, J., Bruyere, C., Wu, W., Vandenberghe, F., Liu, Y., Bourgeois, A., 2009: Update OnWRF-ARWend-to-end Multi-scale FDDA System. 10th WRF Users Workshop. NCAR, Boulder, CO 1.9.

Grell, G. A. and D. Devenyi, 2002: A generalized approach to parameterizing convection combining ensemble and data assimilation techniques. GEOPHYSICAL RESEARCH LETTERS, 29, 1693.

Iacono, M.J., Delamere, J.S., Mlawer, E.J., Shephard, M.W., Clough, S.A., Collins, W.D., 2008. Radiative forcing by long-lived greenhouse gases: calculations with the AER radiative transfer models. J. Geophys. Res. 113, D13103.

Lim, K. S. and S. Y. Hong, 2010: Development of an effective double-moment cloud microphysics scheme with prognostic Cloud Condensation Nuclei (CCN) for weather and climate models, Monthly Weather Review, 138, 1587–1612.

Nakanishi, M., Niino, H., 2006: An improved mellor–yamada level-3 model: its numerical stability and application to a regional prediction of advection fog. Bound. Layer Meteor. 119, 397–407.

Randerson, D. and J. D. Sanders, 2002: Characterization of Cloud-to-Ground Lightning Flashes on the Nevada Test Site. NOAA Tech Memo OAR ARL-242. 29 pp.

Randerson, D., 1999: Five-Year, Warm Season, Cloud-to-Ground Lightning Assessment for Southern Nevada. NOAA Tech Memo OAR ARL-228. 53 pp.

Rutledge, G. K., J. Alpert, and W. Ebisuzaki, 2006: NOMADS: A climate and weather model archive at NOAA. Bull. Amer. Meteor. Soc., 87-3, 327-341. https://nomads.ncep.noaa.gov.

Powers, J.G., Co-authors, 2017. The weather research and forecasting model: overview, system efforts, and future directions. Bull. Am. Meteorol. Soc. 98 (8), 1717–1737.

Stein, A.F., Draxler, R.R., Rolph, G.D., Stunder, B.J.B., Cohen, M.D., Ngan, F., 2015. NOAA's HYSPLIT atmospheric transport and dispersion modeling system. Bull. Am. Meteorol. Soc. 96, 2059–2077.

The NCAR Command Language (Version 6.6.2) [Software]. (2019). Boulder, Colorado: UCAR/NCAR/CISL/TDD. http://dx.doi.org/10.5065/D6WD3XH5Baklanov, A., Grimmond, C.S.B., Carlson, D., Terblanche, D., Tang, X., Bouchet, V., Lee, B., Langendijk, G., Kolli, R.K., Hovsepyan, A., 2018. From urban meteorology, climate and environment research to integrated city services. Urban Climate, 23, 330-341.

Zhang, H., Z. Pu, and X. Zhang, 2013: Examination of Errors in Near-Surface Temperature and Wind from WRF Numerical Simulations in Regions of Complex Terrain. Weather and Forecasting. **28**, 893 – 914.

Table 1. Variable list in the reduced size WRF output files.

Variable short name	**Unit**	**Variable full name**
Times	N/A	time flag
U	ms^{-1}	x-wind component
V	ms^{-1}	y-wind component
W	ms^{-1}	z-wind component
PH	m^2s^{-2}	perturbation geopotential
PHB	m^2s^{-2}	base-state geopotential
T	K	perturbation potential temperature theta-t0
P	Pa	perturbation pressure
PB	Pa	base state pressure
T2	K	2-m temperature
U10	ms^{-1}	x-wind component at 10 m
V10	ms^{-1}	y-wind component at 10 m
TKE_PBL	m^2s^{-2}	turbulent kinetic energy
RAINC	mm	accumulated total cumulus precipitation
RAINNC	mm	accumulated total grid scale precipitation
UST	ms^{-1}	friction velocity
PBLH	m	boundary layer height
HFX	Wm^{-2}	upward heat flux at the surface
LH	Wm^{-2}	latent heat flux at the surface

Table 2. “ID” refers to the Idaho domain and “NV” refers to the Nevada domain.

	South-west corner (km)		**Number of cells**		**Resolution (km)**	**Starting point relative to the mother domain**	
	X-origin	*Y-origin*	*Easting*	*Nothing*		*X-direction*	*Y-direction*
D01	-1332	-1521	149	169	18	1	1
NV02	-450	-450	150	150	6	50	50
NV03	-150	-150	150	150	2	51	51
ID02	-252	-288	150	150	6	61	101
ID03	60	60	168	156	2	53	53

Table 3. Physics options used in the WRF forecasting system.

	D01	**NV02 and ID02**	**NV03 and ID03**
Grid spacing (km)	18	6	2
IC/BC	GFS 0.5 deg	D01 nestdown	NV02 or ID02 nestdown
Microphysics	WSM 6-class graupel (Lim and Hong, 2010)		
Cumulus	Grell 3D ensemble (Grell and Devenyi, 2002)		
Radiation	RRTMG (Iacono et al. 2008)		
PBL	MYNN 2.5 level (Nakanishi and Niino, 2006)		
Surface scheme	MYNN (Nakanishi and Niino, 2006)		
Land-surface model	Noah LSM (Chen and Dudhia, 2001)		
Nudging	Analysis nudging (Deng et al. 2009)		Analysis nudging (no PBL wind)
Time step (sec)	60	30	10

Table 4. The list of stations used for skew-T diagram and meteogram figures.

Area	Station name	Latitude	Longitude	Elevation (m, MSL)
Nevada	A22AD	36.624352	-116.022423	1001.4
	A01AB	37.063098	-116.053987	1244.9
	A12AG	37.186192	-116.215635	2267.5
	A25AH	36.784665	-116.289558	1048.2
	NFO	36.2100	-115.1400	---
	KLAS	36.0840	-115.1537	---
Idaho	CFA	43.533	-112.948	1512
	MFC	43.594	-112.652	1567
	SMC	43.860	-112.730	1460
	IDA	43.504	-112.050	1441

Table 5. The list of mesonet stations in southern Nevada.

#	Station name	Latitude	Longitude	Elevation (m)
1	A01AA	37.00365	-116.0597	1214.6
2	A01AB	37.0631	-116.054	1244.9
3	A04AA	37.09672	-116.0885	1288.1
4	A05AA	36.80175	-115.9663	943.8
5	A05AB	36.8476	-115.9534	962.9
6	A06AA	36.89371	-116.0389	1103.5
7	A06AE	36.93775	-116.0377	1197.3
8	A09AB	37.12332	-116.0429	1274
9	A10AA	37.18599	-116.0444	1330.8
10	A12AF	37.19569	-116.1601	1619.8
11	A12AG	37.18619	-116.2156	2267.5
12	A12AI	36.67207	-116.404266	2753.0
13	A14AA	36.96756	-116.1811	1441.7
14	A18AA	37.1515	-116.3952	1672.5
15	A18AB	37.10418	-116.3138	1542.2
16	A20AA	37.25655	-116.4355	2004
17	A20AB	37.34499	-116.569	1710
18	A22AD	36.62435	-116.0224	1001.4
19	A23AA	36.65697	-116.0031	1121.3
20	A25AH	36.78467	-116.2896	1048.1
21	A25AI	36.67207	-116.4043	838.9
22	A26AA	36.81212	-116.1611	1309.7
23	A27AA	36.77006	-116.1047	1391.3
24	OYMAB	36.85228	-116.4664	1481.3

Table 6. The list of mesonet stations in southeastern Idaho.

#	Station name	Latitude	Longitude	Elevation (m)
1	BAS	43.67753	-113.006	1493.52
2	CFA (690)	43.53262	-112.9477	1508.76
3	DEA	43.62507	-113.0598	1556.918
4	EBR	43.59413	-112.6517	1567.586
5	GRI	43.5897	-112.9399	1492.606
6	LOF	43.85977	-112.7303	1459.992
7	LOS	43.54868	-113.0099	1518.818
8	NRF	43.64787	-112.9112	1477.366
9	PBF	43.54748	-112.8697	1496.568
10	ROV	43.7206	-112.5296	1526.438
11	RWM	43.50343	-113.046	1531.62
12	SAN	43.77967	-112.7582	1469.136
13	TRA	43.58463	-112.9687	1504.798
14	ABE	42.95493	-112.8245	1338.682
15	ARC	43.62455	-113.2971	1612.392
16	ATO	43.44373	-112.8157	1541.678
17	BLK	43.18985	-112.3332	1377.696
18	BLU	44.075	-112.842	1731.264
19	COX (BIG)	43.29417	-113.1813	1584.96
20	CRA	43.42918	-113.5383	1827.581
21	DUB	44.24238	-112.2018	1665.732
22	FOR	43.022	-112.412	1356.97
23	HAM	44.00742	-112.2388	1476.146
24	HOW	43.78412	-112.9773	1467.612
25	IDA	43.50413	-112.0501	1435.303
26	KET	43.54757	-112.3263	1581.912
27	MIN	42.80442	-113.5897	1306.068
28	MON	44.01537	-112.5359	1462.126
29	RIC	43.0606	-114.1346	1315.212
30	ROB	43.74352	-112.1211	1450.848
31	SUG	43.89658	-111.7376	1491.996
32	SUM	43.39633	-113.0219	2309.165
33	TAB	43.31868	-112.6918	1441.704
34	TER	43.84168	-112.4183	1460.602

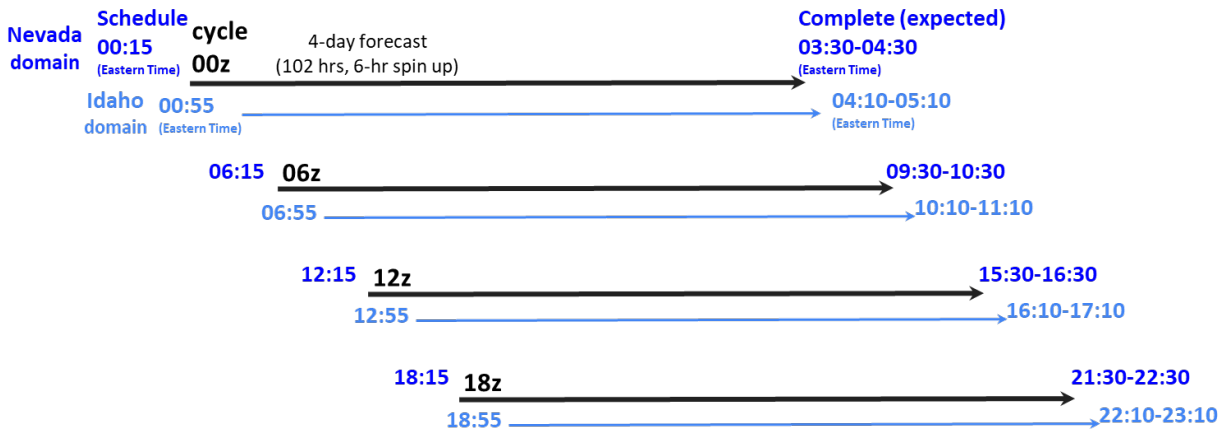

Figure 1. The nominal operating schedule for the Nevada domain (darker blue) and the Idaho domain (lighter blue). The start of the NV and ID WRF forecasts must wait until the GFS data product is completed and so, are started 4-5 hours after the stated cycle time, i.e., the 00z cycle WRF forecast starts at 04:15 UTC.

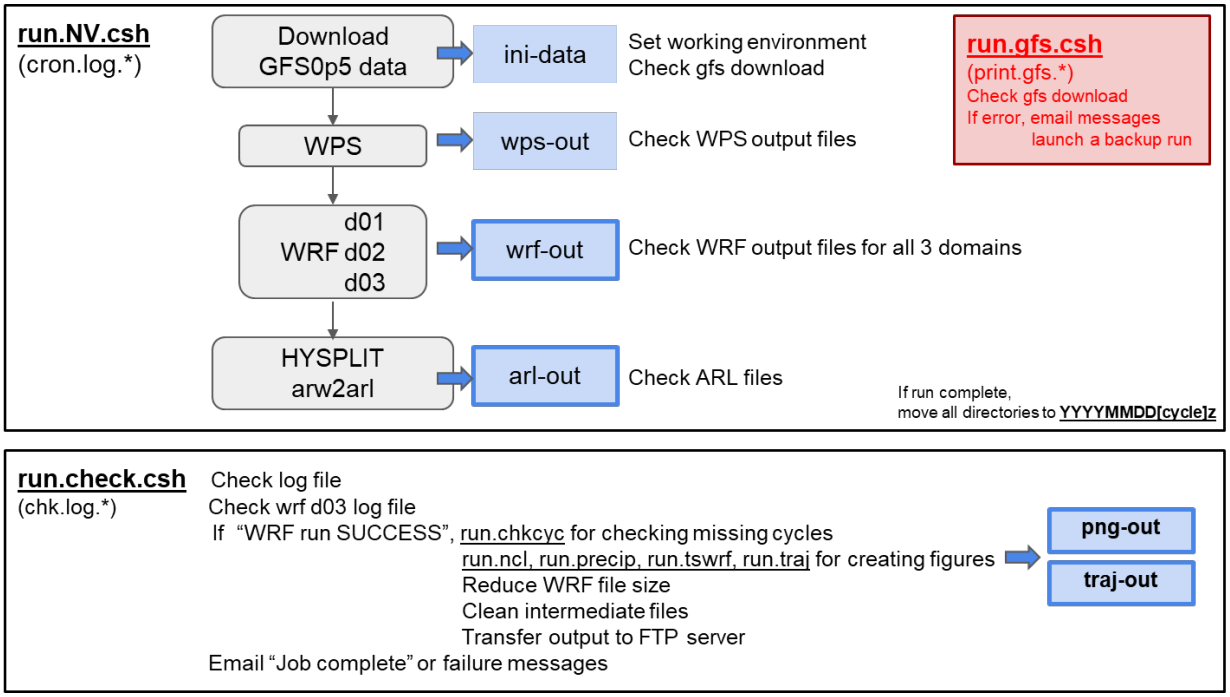

Figure 2. Schematic of the two main scripts used in the WRF forecasting system. The blue boxes are output directories and the grey boxes are the processes that are run to produce output. The "ini-data" and "wps-out" directories are removed once a WRF simulation is complete.

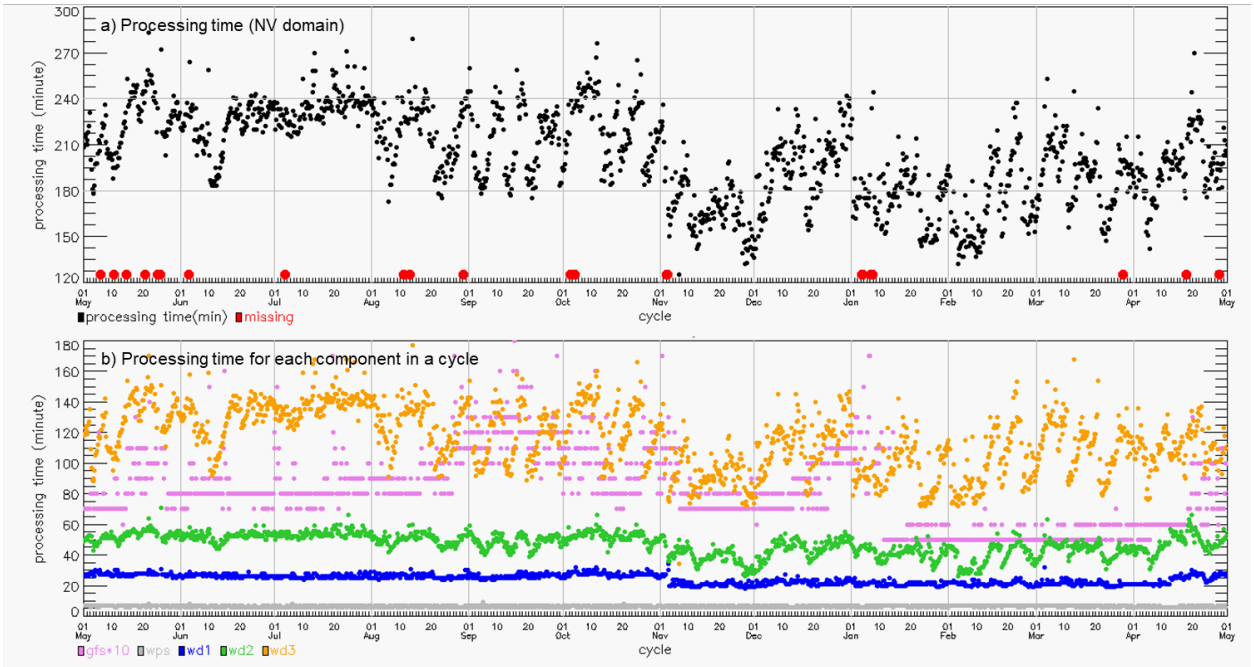

Figure 3. Time series of a) the processing time to complete one cycle for the NV domain; b) the processing time for each component. The big red dots in a) refer to incomplete runs. The labels in b) "gfs", wps, wd1, wd2, and wd3 refer to GFS download (minutes*10), WRF preprocessing system, WRF run for D01, D02, and D03, respectively.

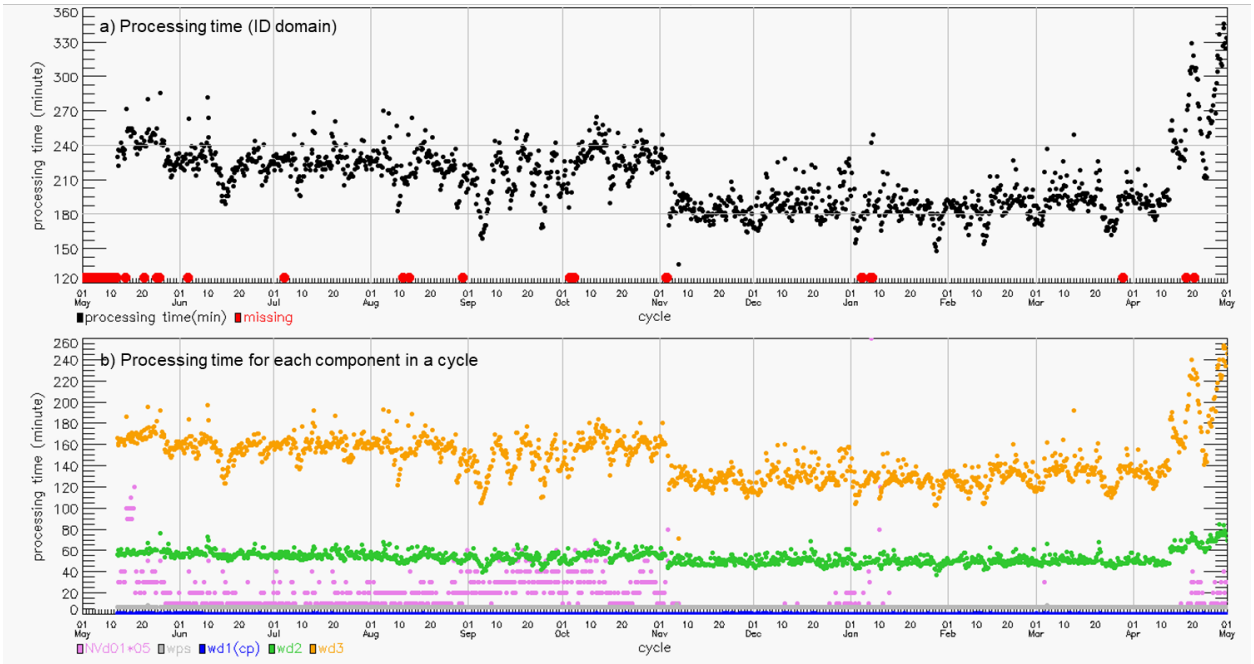

Figure 4. The same as Figure 3 but for the ID domain. Note that the ID run uses wd1 output from the NV run and pink dots indicate when the ID run starts, how long (minutes*5) it waits for the NV wd1 files to become available.

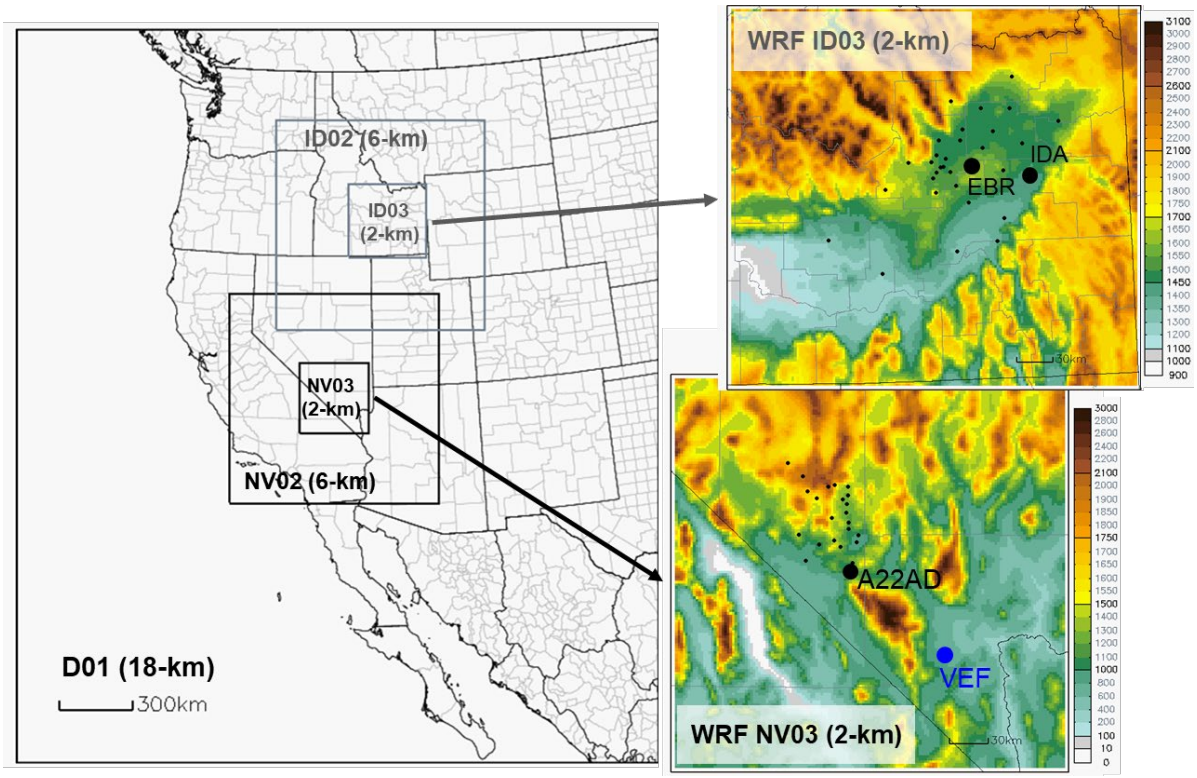

Figure 5. The WRF simulation domains for the Nevada and Idaho area. Black dots are mesonet sites (with the larger black dots representing specific mesonet sites for which additional analysis was done, as discussed in the text) and the blue dot is a radiosonde site. The background represents model terrain height. Unit: meter.

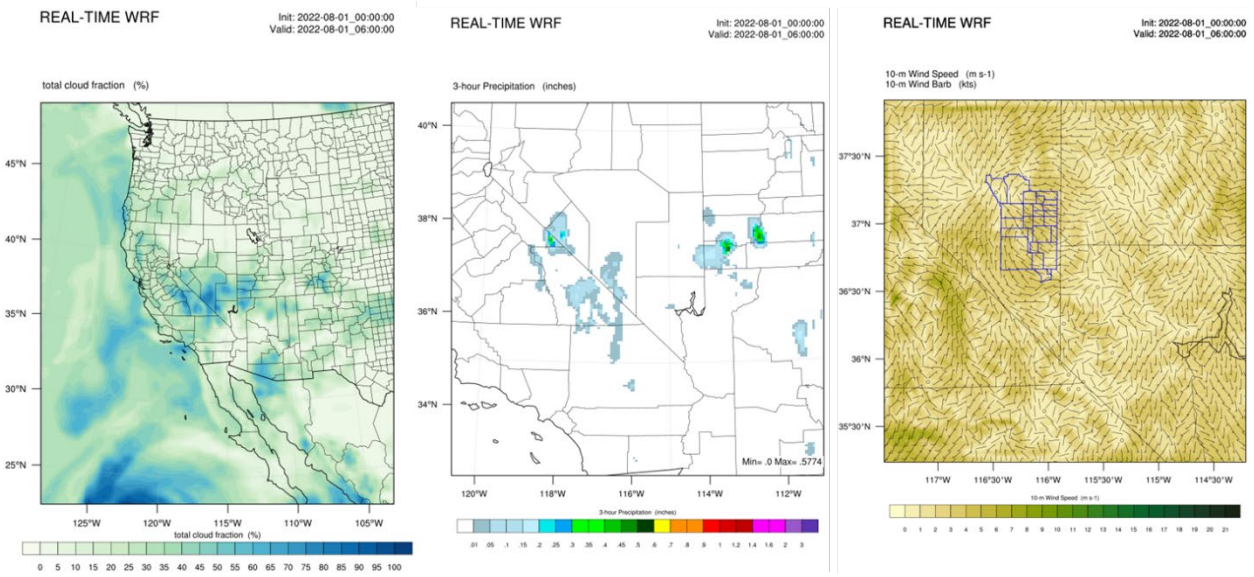

Figure 6. Examples of surface plots: the total cloud fraction for D01 (left), the 3-hour precipitation for NV02 (middle), and the 10-m wind speed and barb for NV03 (right).

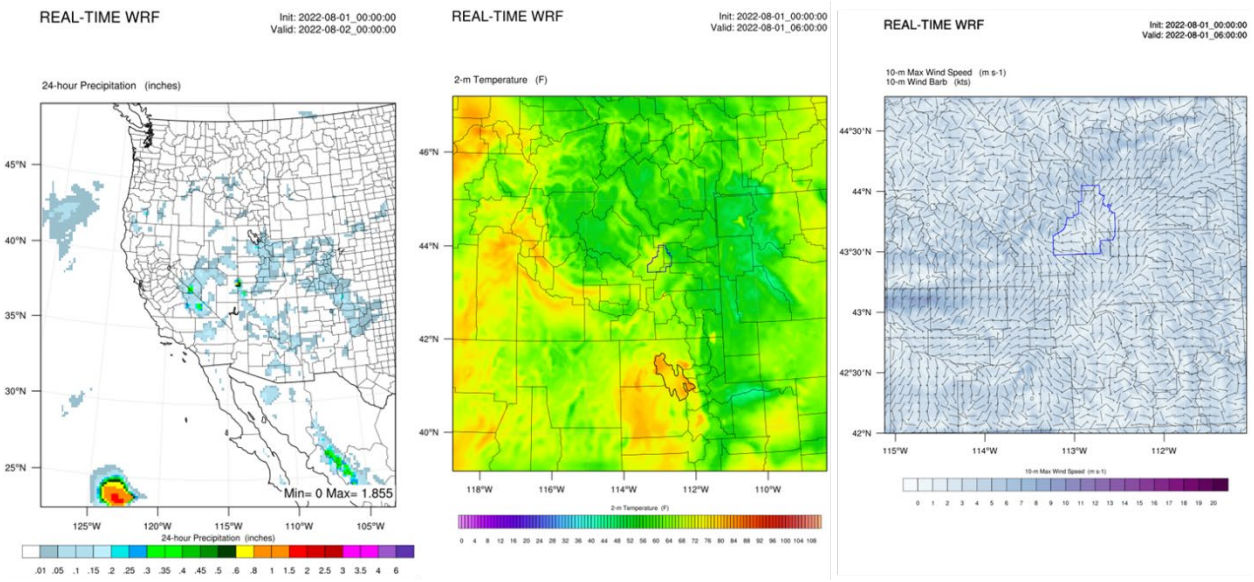

Figure 7. Examples of surface plots: the 24-hour precipitation for D01 (left), the 2-m temperature for ID02 (middle), and the 10-m maximum wind speed and 10-m wind barb for ID03 (right).

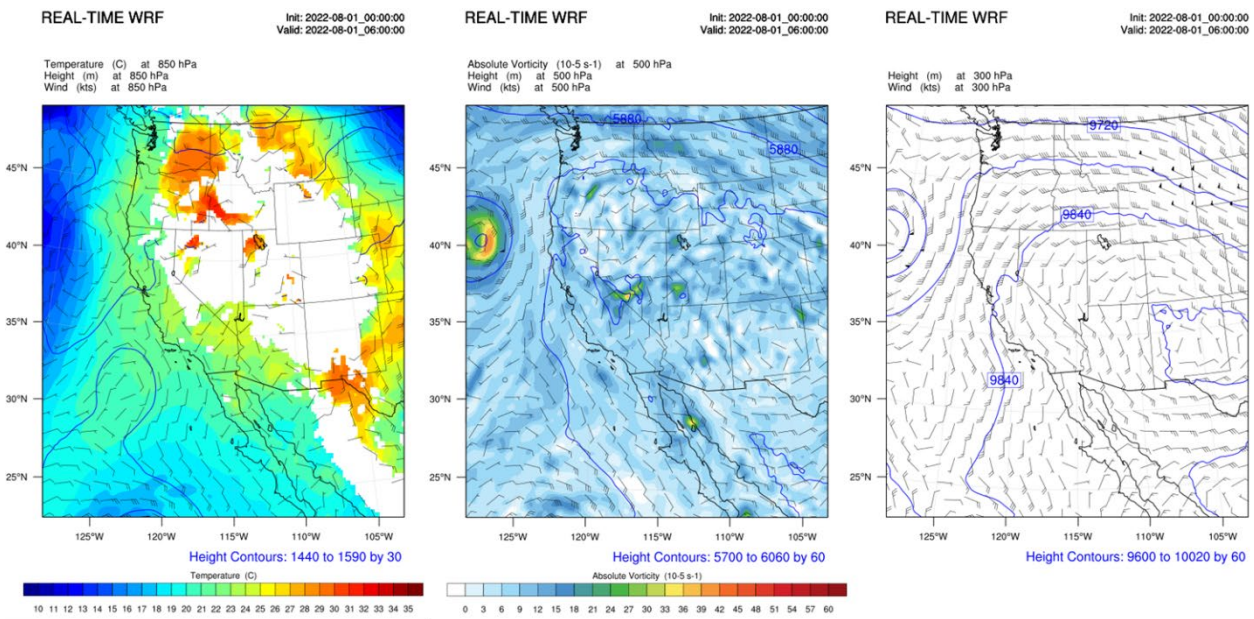

Figure 8. Examples of upper level plots: the 850 mb weather map (left), the 500 mb weather map (middle), and the 300 mb weather map (right).

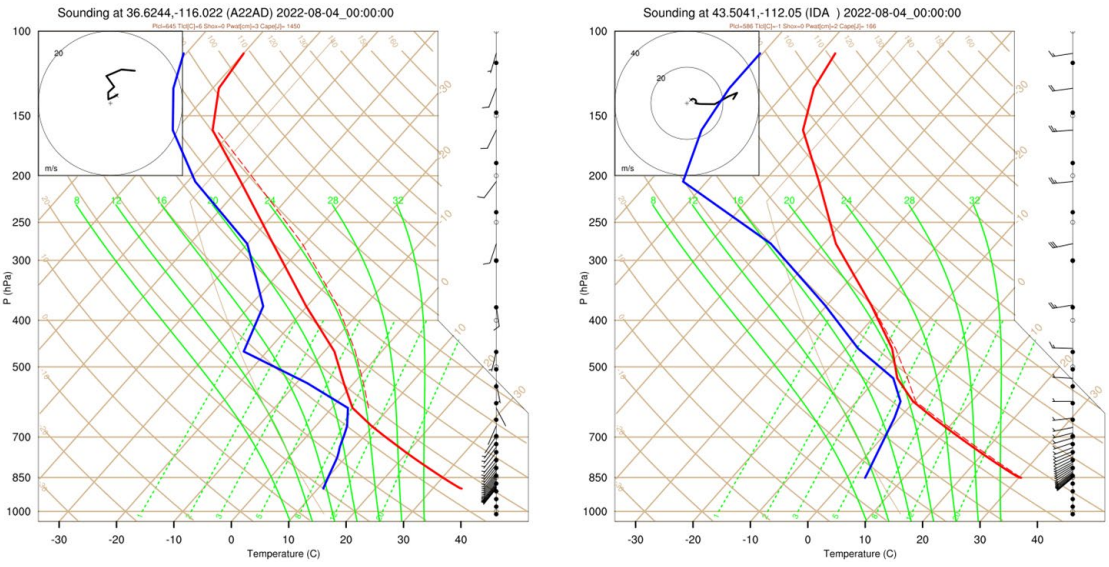

Figure 9. Examples of skew-t plots at stations A22AD (left) and IDA (right).

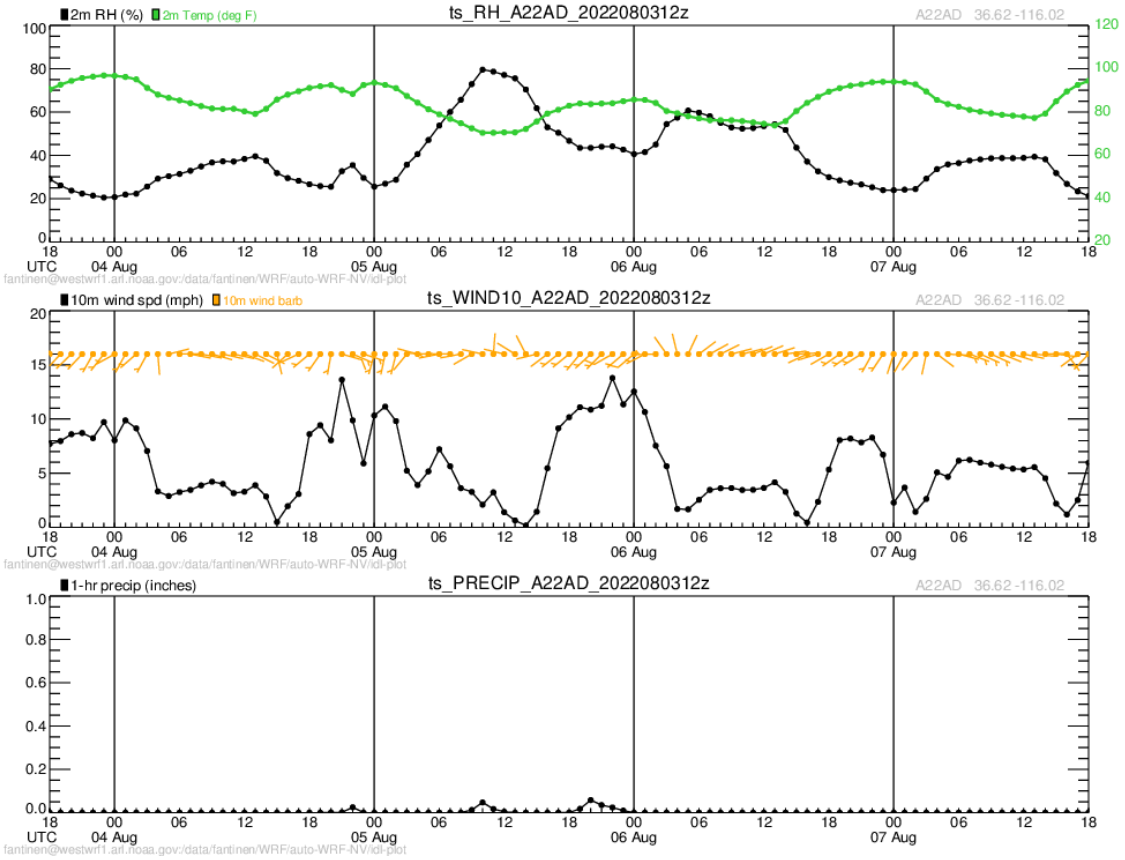

Figure 10. An example of time series plot at the station A22AD.

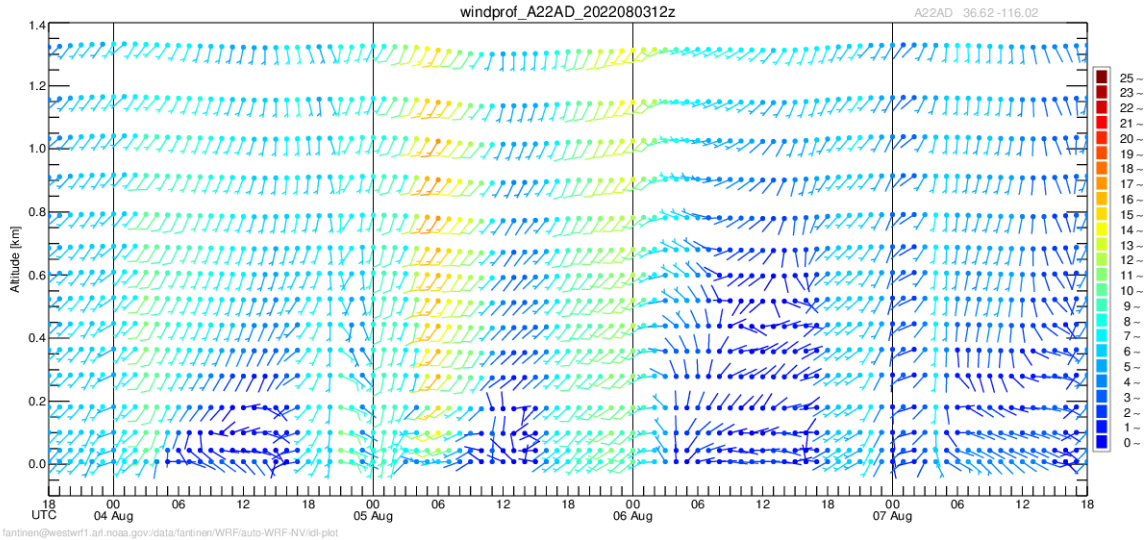

Figure 11. An example of the wind profile time series plot at the station IDA.

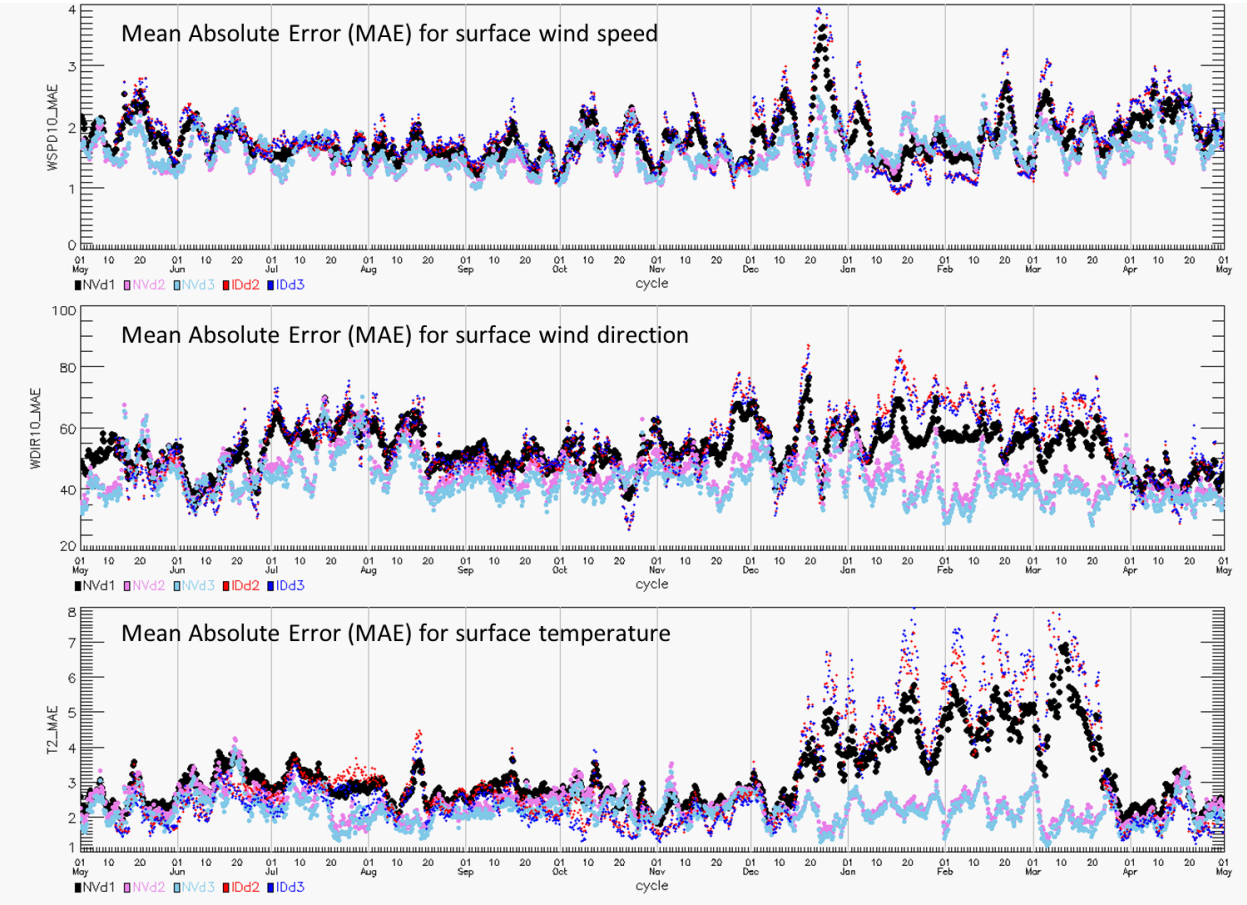

Figure 12. Mean absolute error between WRF forecasts and mesonet observations for wind speed (ms^{-1}), wind direction (degrees), and temperature (degrees Celsius) during May 1st, 2021 to April 30th, 2022. The different color-coded symbols are for the different forecast domains shown in Figure 5.

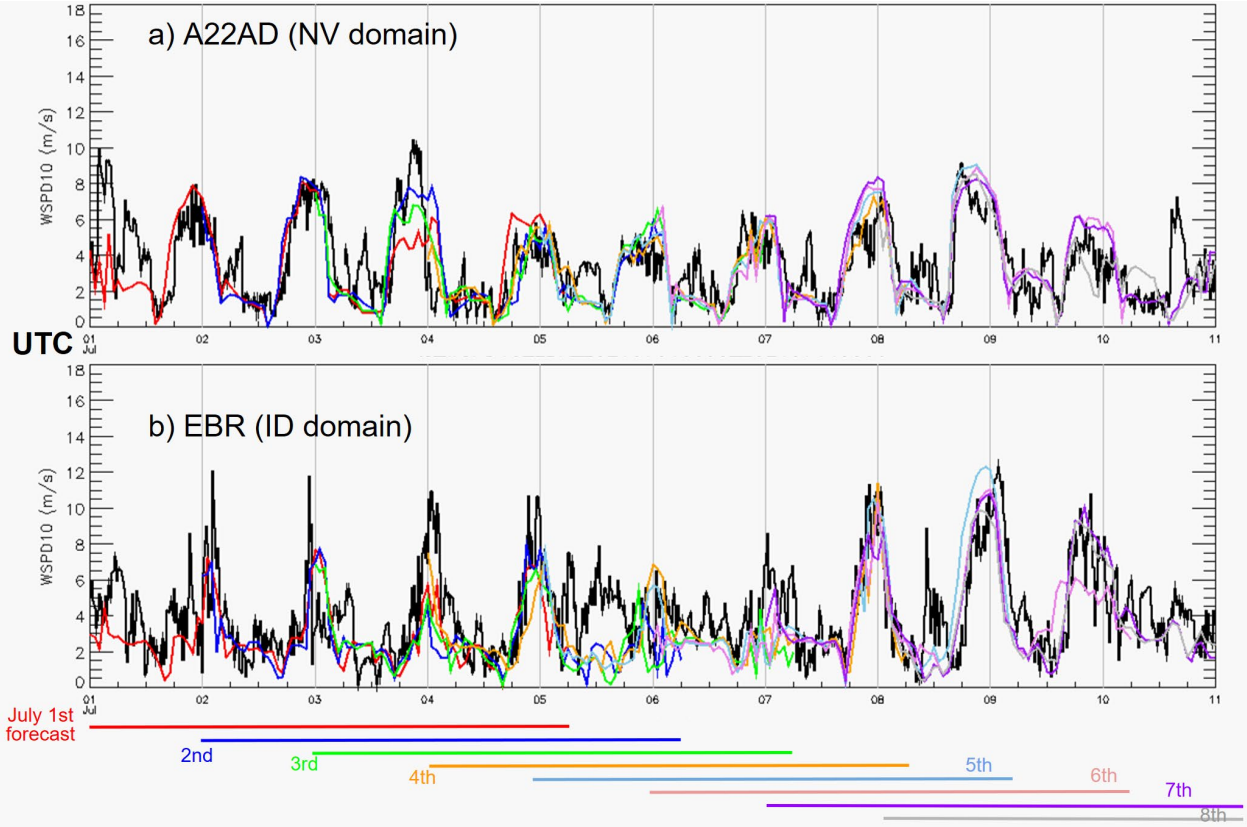

Figure 13. Time series of surface wind speed at station a) A22AD and b) EBR from the July 1st – 8th, 2020, 00z cycle forecasts, compared with observations in 15-minute intervals (black line).

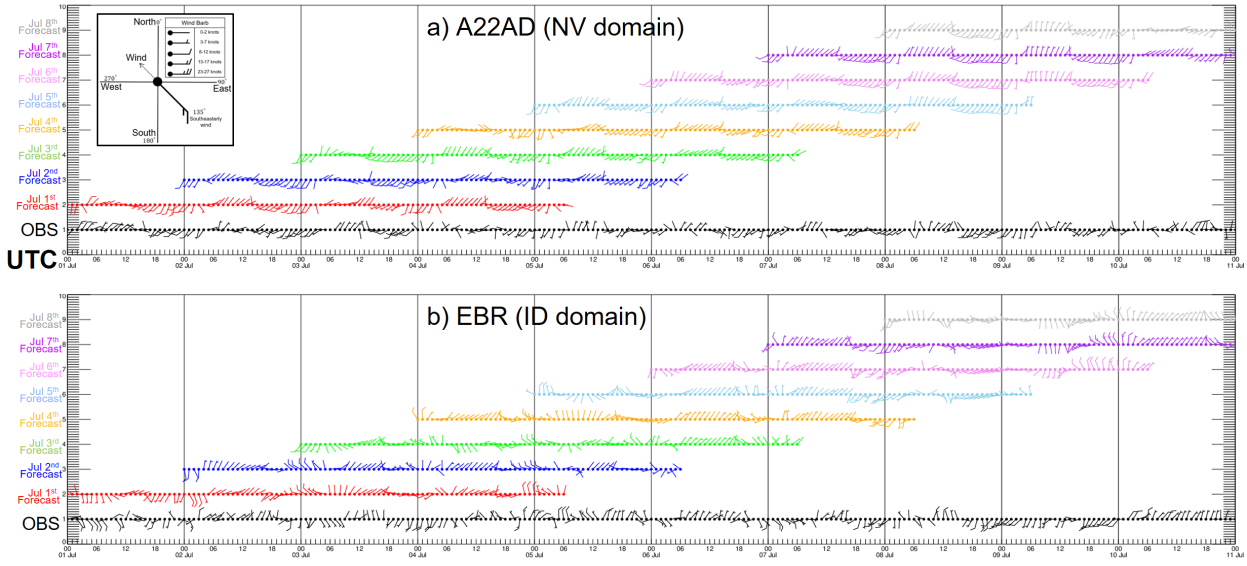

Figure 14. Surface wind barbs at station a) AA2AD and b) EBR from July 1st – 8th, 2020, 00z cycle forecasts, compared with hourly observations.

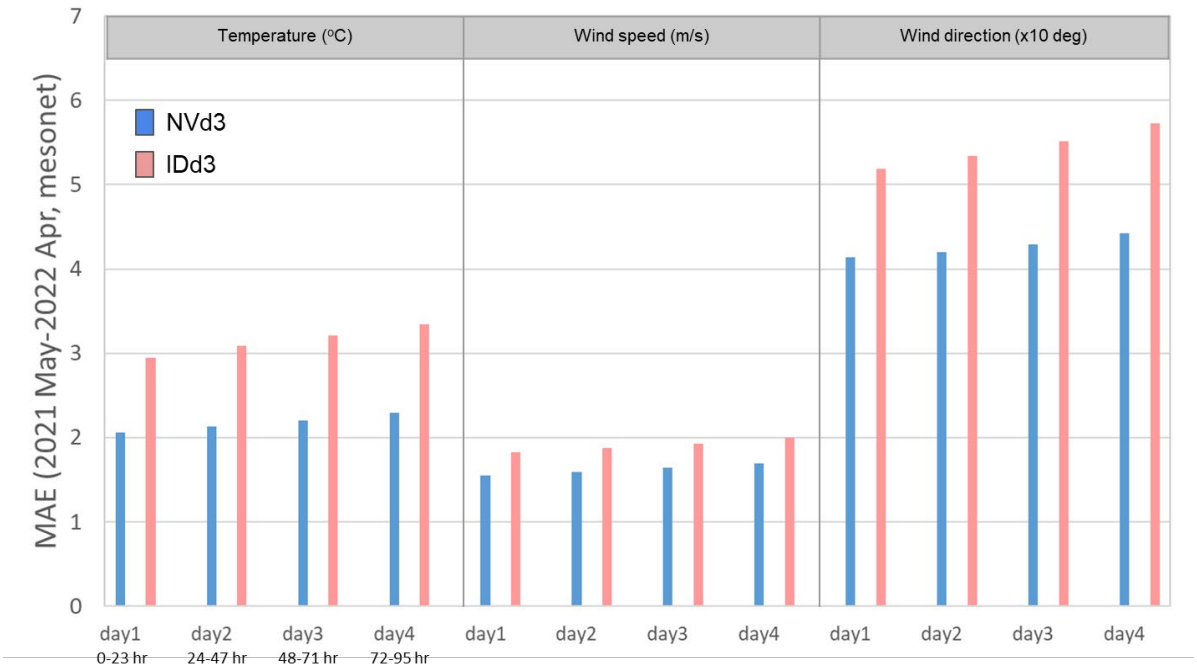

Figure 15. Mean Absolute error computed for the different forecast days during May 1st, 2021 to April 30th, 2022.

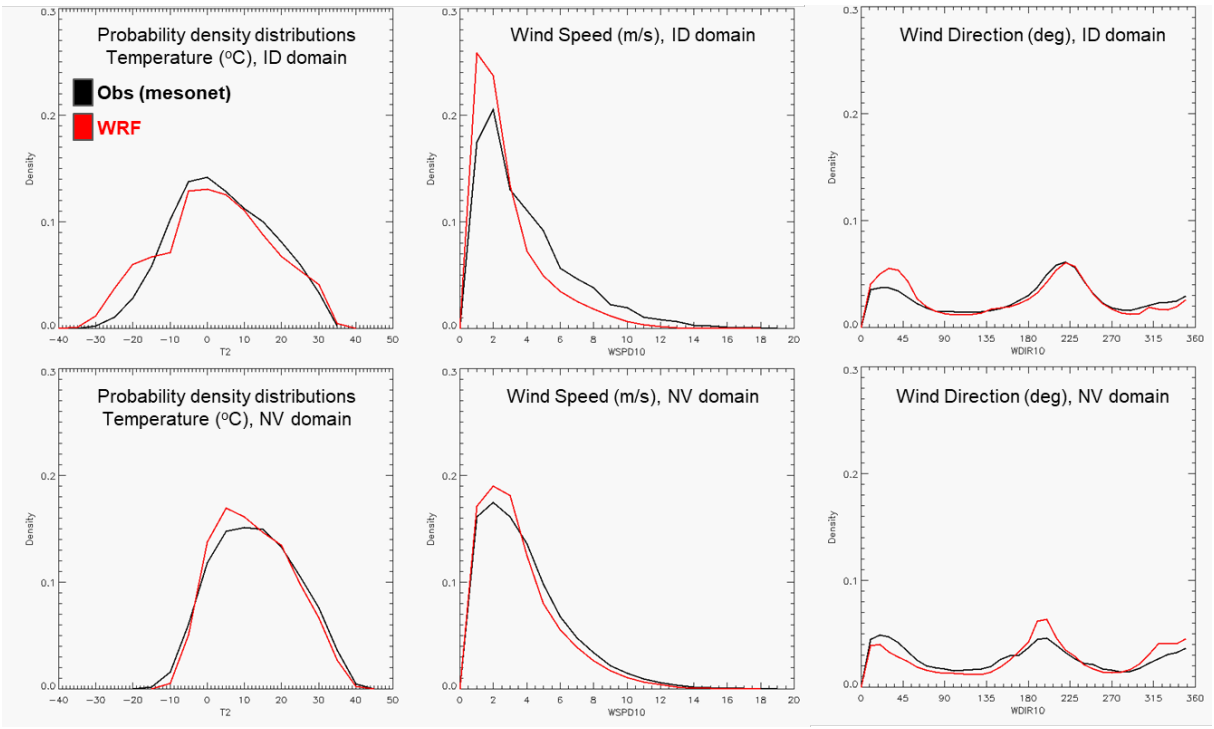

Figure 16. Comparison of observed (black line) and model (red line) surface temperature, wind speed, and wind direction probability density distribution during May 1st, 2021 to April 30th, 2022. The observations are mesonet data in the NV and ID domain. The histogram intervals are 5 degrees Celsius for temperature, 1 ms^{-1} for wind speed, and 10 degrees for wind direction.

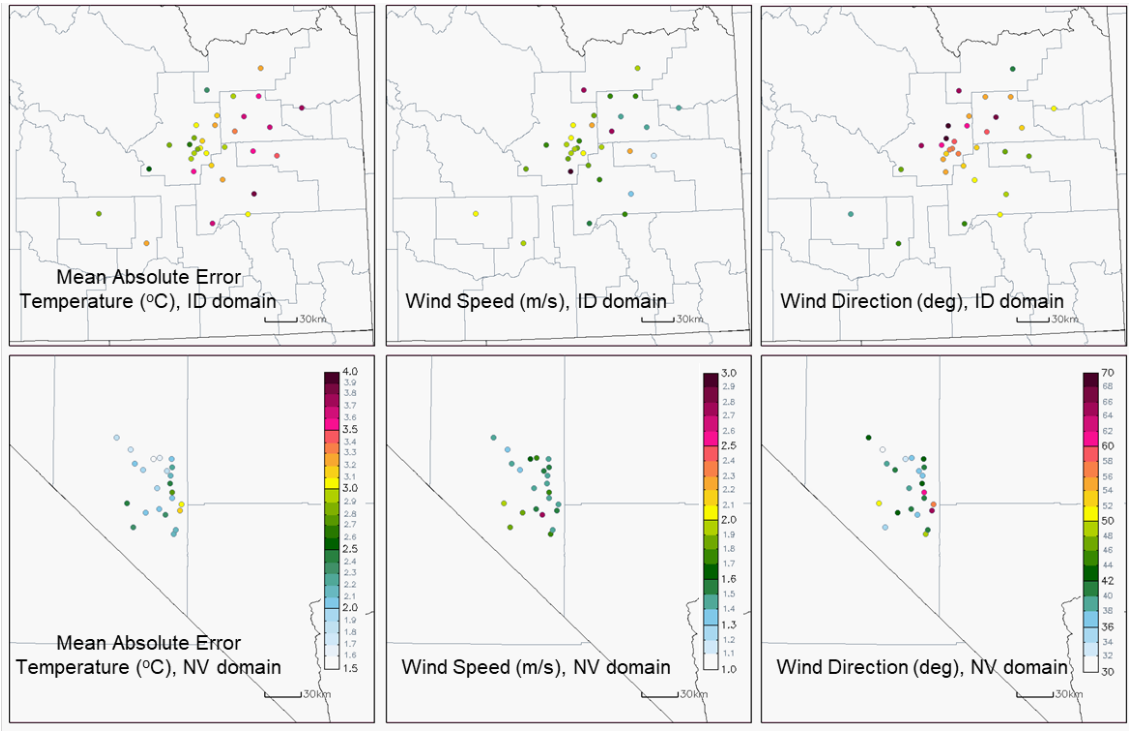

Figure 17. Mean absolute error for each station for surface temperature, wind speed, and wind direction during May 1st, 2021 to April 30th, 2022.

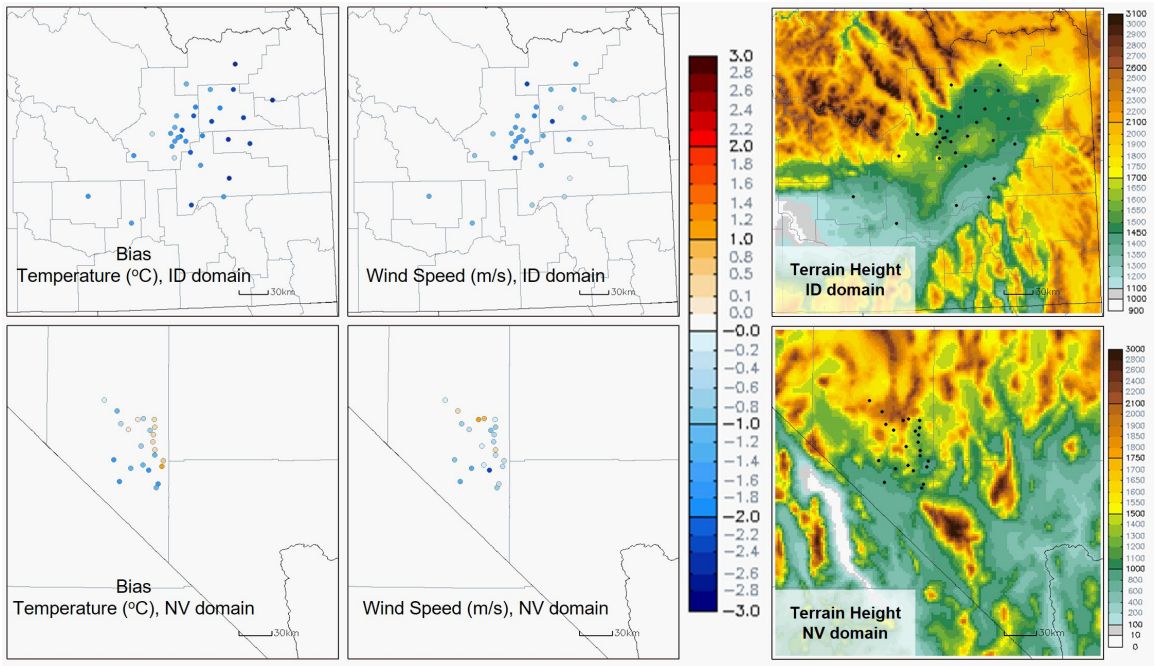

Figure 18. Bias for each station for temperature and wind speed during May 1st, 2021 to April 30th, 2022. The left row is the spatial plot of model terrain height (unit: meter). Black dots are mesonet stations while the red dot is a radiosonde site.

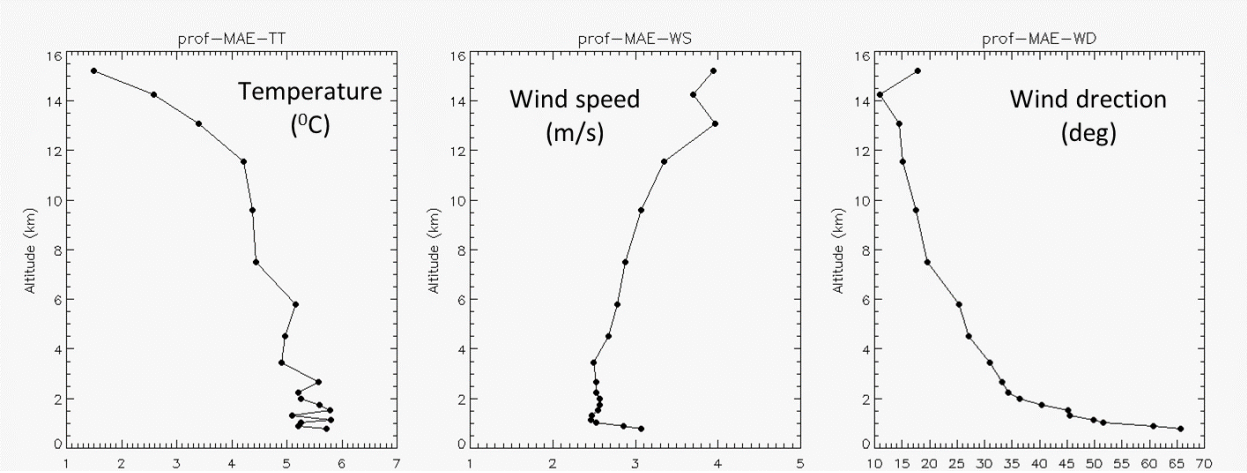

Figure 19. Vertical profiles of mean absolute error for temperature, wind speed, and wind direction derived from the VEF radiosonde and the NV-domain WRF forecast during May 1st, 2021 to April 30th, 2022.